

# Time Developing Flow in a Parallel Plate Channel

AME 531 - Numerical Methods in Fluid Mechanics and Heat Transfer

Theo Altneu

University of Arizona

September 16, 2025

---

## Abstract

This study investigates the time evolution of a viscous, incompressible fluid flow between two infinite parallel plates under a constant pressure gradient. The Navier-Stokes equation is simplified to a one-dimensional form and nondimensionalized to obtain a more general representation of the problem. The analytical solution is derived using separation of variables and Fourier series techniques, resulting in a solution expressed as an infinite sum of eigenfunctions. In addition to the exact analytical solution, three numerical methods are implemented and compared: implicit Euler, explicit Euler and the classical fourth-order Runge-Kutta method. Results demonstrate that all three methods correctly captured the transient evolution of the velocity profile and asymptotic approach to the steady-state parabolic distribution. The implicit method showed reliable stability and acceptable accuracy, even for relatively large timesteps. Grid sensitivity analysis revealed that both spatial and temporal resolutions significantly impact numerical accuracy. The study concludes that implicit methods offer robustness, while higher-order schemes like the 4th-Order Runge-Kutta can be advantageous when sufficient resolution and stability conditions are maintained.

## 1 Introduction

The study of unsteady flow in simple geometries, such as a parallel plate channel, provides a foundational understanding of fluid behavior during transient development. These flows arise in numerous practical engineering scenarios, such as the startup of pipeline systems. Typically, the assumption of fully developed flow is invalid, and it becomes essential to solve the governing equations of fluid motion with respect to time.

This report focuses on the time development of a viscous, incompressible fluid flow between two infinite parallel plates under a constant pressure gradient. The Navier-Stokes equation is simplified to a one-dimensional form and nondimensionalized to obtain a more general representation of the problem. The analytical solution is derived using separation of variables and Fourier series techniques, resulting in a solution expressed as an infinite sum of eigenfunctions.

In addition to the exact analytical solution, three numerical methods are implemented and compared: implicit Euler, explicit Euler, and the classical 4th-order Runge-Kutta method (RK4). These methods are evaluated for their accuracy, convergence to the steady-state parabolic profile, and stability under varying timestep and grid spacing conditions. Key quantities of interest such as the dimensionless velocity profile, volumetric flow rate, and wall shear stress are computed to compare the behavior and performance of each method.

## 2 Problem Formulation

In this report, the time evolution of flow in a parallel plate channel is considered. The plates are a distance of  $2h$  apart. Due to symmetry about the centerline at  $y = 0$ , only the upper half of the domain is considered in the analysis. The fluid is considered initially at rest and

then evolves to a steady-state solution.

$$\frac{\partial u}{\partial t} = -\frac{1}{\rho} \frac{dp}{dx} + \nu \frac{\partial^2 u}{\partial y^2} \quad (1)$$

Equation (1) is the governing Navier-Stokes equation simplified for this type of flow problem, where  $dp/dx$  is a constant pressure gradient. The boundary and initial conditions are defined by (2), (3) and (4).

$$u(y, 0) = 0 \quad (2)$$

$$\frac{\partial u}{\partial y}(0, t) = 0 \quad (3)$$

$$u(h, t) = 0 \quad (4)$$

The first step is to nondimensionalize (1), the initial condition (2), and the boundary conditions (3) and (4) by using the dimensionless parameters (5), (6), and (7).

$$y^* = \frac{y}{h} \quad (5)$$

$$u^* = \frac{\rho \nu u}{-h^2 \frac{dp}{dx}} \quad (6)$$

$$t^* = \frac{\nu t}{h^2} \quad (7)$$

Substituting the dimensionless variables into Equation (1) yields

$$\frac{\left(\frac{-h^2 \frac{dp}{dx}}{\rho \nu}\right) \partial u^*}{\left(\frac{h^2}{\nu}\right) \partial t^*} = -\frac{1}{\rho} \frac{dp}{dx} + \nu \frac{\left(\frac{-h^2 \frac{dp}{dx}}{\rho \nu}\right) \partial^2 u^*}{h^2 \partial y^{*2}} \quad (8)$$

Then by dividing both sides by the coefficient, the final dimensionless Navier-Stokes equation is obtained.

$$\frac{\partial u^*}{\partial t^*} = 1 + \frac{\partial^2 u^*}{\partial y^{*2}} \quad (9)$$

The non-dimensional initial condition becomes

$$u(y, 0) = 0 \rightarrow u^*(y^*, 0) = 0 \quad (10)$$

The non-dimensional boundary conditions become

$$\frac{\partial u}{\partial y}(0, t) = 0 \rightarrow \frac{\partial u^*}{\partial y^*}(0, t^*) = 0 \quad (11)$$

$$u(h, t) = 0 \rightarrow u^*(1, t^*) = 0 \quad (12)$$

To find the exact solution to the dimensionless Navier-Stokes equation, Equation (9) can be solved by separation of variables, assuming

$$u^*(y^*, t^*) = Y(y^*)T(t^*) \quad (13)$$

First, consider the homogeneous equation

$$\frac{\partial u^*}{\partial t^*} = \frac{\partial^2 u^*}{\partial y^{*2}} \quad (14)$$

Substituting Equation (13) into Equation (14) leads to

$$Y(y^*) \dot{T}(t^*) = Y''(y^*) T(t^*) \quad (15)$$

$$\frac{Y''}{Y} = \frac{\dot{T}}{T} = \lambda \quad (16)$$

From which the spatial ODE can be found as

$$Y'' + \lambda^2 Y = 0 \quad (17)$$

Which is assumed to have the solution form of

$$Y(y^*) = A \cos \lambda y^* + B \sin \lambda y^* \quad (18)$$

Applying the boundary conditions (11) and (12), the coefficients from (18) can be determined.

$$Y'(0) = 0 \rightarrow B = 0 \quad (19)$$

$$Y(1) = 0 \rightarrow A \cos \lambda = 0 \quad (20)$$

For the non-trivial solution,  $A \neq 0$ , so we assume the value of  $\lambda$  to be

$$\lambda_n = (2n - 1) \frac{\pi}{2}, n = 1, 2, 3... \quad (21)$$

Therefore, the solution of Equation (14) can be written as

$$u^*(y^*, t^*) = \sum_{n=1}^{\infty} T_n(t^*) \cos \lambda_n y^* \quad (22)$$

To solve for the time-dependent coefficients  $T_n$ , we substitute the assumed solution form from Equation (22) into the non-dimensional governing equation (9):

$$\sum_{n=1}^{\infty} \dot{T}_n \int_0^1 \cos \lambda_m y^* \cos \lambda_n y^* dy = \int_0^1 \cos \lambda_m y^* dy - \sum_{n=1}^{\infty} \lambda_n^2 T_n \int_0^1 \cos \lambda_m y^* \cos \lambda_n y^* dy \quad (23)$$

$$\frac{1}{2} \dot{T}_m = \frac{1}{\lambda_m} \sin \lambda_m - \frac{1}{2} \lambda_m^2 T_m \quad (24)$$

$$\dot{T}_m + \lambda_m^2 T_m = \frac{2}{\lambda_m} (-1)^{m+1} \quad (25)$$

$$\frac{d}{dt} (T_m e^{\lambda_m^2 t^*}) = \frac{2}{\lambda_m} (-1)^{m+1} e^{\lambda_m^2 t^*} \quad (26)$$

$$T_m e^{\lambda_m^2 t^*} = \frac{2}{\lambda_m^3} (-1)^{m+1} e^{\lambda_m^2 t^*} + C \quad (27)$$

---


$$T_m(t^*) = \frac{2}{\lambda_m^3}(-1)^{m+1} + Ce^{-\lambda_m^2 t^*} \quad (28)$$

Applying the initial condition from Equation (10) to Equation (28) allows for the constant of integration  $C$  to be calculated.

$$T_m(0) = 0 = \frac{2}{\lambda_m^3}(-1)^{m+1} + C \rightarrow C = -\frac{2}{\lambda_m^3}(-1)^{m+1} \quad (29)$$

$$T_m(t^*) = \frac{2(-1)^{m+1}}{\lambda_m^3}(1 - e^{-\lambda_m^2 t^*}) \quad (30)$$

By plugging Equation (30) into Equation (22), the exact solution is obtained.

$$u^*(y^*, t^*) = 2 \sum_{n=1}^{\infty} \frac{(-1)^{n+1}}{\lambda_n^3} (1 - e^{-\lambda_n^2 t^*}) \cos \lambda_n y^* \quad (31)$$

where

$$\lambda_n = (2n - 1) \frac{\pi}{2}, \quad n = 1, 2, 3, \dots \quad (32)$$

The flow rate as a function of time and the wall shear stress as a function of time are also required for later analysis. Flow rate is defined by

$$Q(t) = \int u(y, t) dy \quad (33)$$

Which can be expressed in the dimensionless form

$$Q(t^*) = \int u^*(y^*, t^*) dy^* \quad (34)$$

The flow rate can be calculated by

$$Q(t^*) = 2 \int_0^1 u^*(y^*, t^*) dy^* = 4 \sum_{n=1}^{\infty} \frac{(-1)^{n+1}}{\lambda_n^3} (1 - e^{-\lambda_n^2 t^*}) \int_0^1 \cos \lambda_n y^* dy^* \quad (35)$$

Computing the inner integral

$$\int_0^1 \cos \lambda_n y^* dy^* = \frac{\sin \lambda_n}{\lambda_n} = \frac{(-1)^{n+1}}{\lambda_n} \quad (36)$$

By simplifying the equation, the flow rate for the exact solution becomes

$$Q(t^*) = 4 \sum_{n=1}^{\infty} \frac{1 - e^{-\lambda_n^2 t^*}}{\lambda_n^4} \quad (37)$$

Wall shear stress is defined by

$$\tau = - \left. \frac{\partial u}{\partial y}(y, t) \right|_{wall} \quad (38)$$

Which can be expressed in the dimensionless form

$$\tau = -\frac{\partial u^*}{\partial y^*}(y^*, t^*) \Big|_{wall} \quad (39)$$

Where the wall is at  $y = 1$ , as given by the boundary condition Equation (12). The wall shear stress can be calculated by first computing the derivative of  $u^*$  with respect to  $y^*$ .

$$\frac{\partial u^*}{\partial y^*} = 2 \sum_{n=1}^{\infty} \frac{(-1)^{n+1}}{\lambda_n^3} (1 - e^{-\lambda_n^2 t^*}) \frac{d}{dy} \cos \lambda_n y^* \quad (40)$$

Plugging in  $y^* = 1$  and simplifying leads to

$$\frac{\partial u^*}{\partial y^*} \Big|_{y^*=1} = -2 \sum_{n=1}^{\infty} \frac{1}{\lambda_n^2} (1 - e^{-\lambda_n^2 t^*}) \quad (41)$$

So the wall shear stress of the exact solution is found to be

$$\tau = 2 \sum_{n=1}^{\infty} \frac{1}{\lambda_n^2} (1 - e^{-\lambda_n^2 t^*}) \quad (42)$$

### 3 Numerical Formulation

The numerical solution must be found using an implicit method, an explicit method, and a RK4 method. The implicit Euler and explicit Euler methods were chosen for their ease of implementation. The definition of the dimensionless time-stepping parameter is

$$r = \frac{\Delta t^*}{(\Delta y^*)^2} \quad (43)$$

Uniform grids are used for all numerical methods in this section.

#### 3.1 Implicit Euler Method

To develop the implicit Euler method to solve Equation (9) with the initial condition in Equation (10) and boundary conditions in Equations (11) and (12), the domain must first be discretized. Let  $N_y$  be the number of spatial intervals,  $\Delta y^* = \frac{1}{N_y}$  where  $j = 0, 1, \dots, N_y$ , and  $N_t$  is the number of time steps with  $\Delta t^* = \frac{T}{N_t}$  where  $T$  is when the solution reaches its steady state and  $n = 0, 1, \dots, N_t$ . Therefore,  $y_j^*$ ,  $t_n^*$  and  $u_j^n$  can be defined as

$$y_j^* = j \Delta y^* \quad (44)$$

$$t^* = n \Delta t^* \quad (45)$$

$$u_j^n \approx u^*(y_j^*, t_n^*) \quad (46)$$

A backward difference scheme in time and a central difference scheme in space are applied.

$$\frac{\partial u^*}{\partial y^*} \Big|_j^{n+1} \approx \frac{u_j^{n+1} - u_j^n}{\Delta t^*} \quad (47)$$

---


$$\frac{\partial^2 u^*}{\partial y^{*2}} \Big|_j^{n+1} \approx \frac{u_{j+1}^{n+1} - 2u_j^{n+1} + u_{j-1}^{n+1}}{(\Delta y^*)^2} \quad (48)$$

Substituting Equation (47) and (48) into Equation (9) leads to

$$\frac{u_j^{n+1} - u_j^n}{\Delta t^*} = 1 + \frac{u_{j+1}^{n+1} - 2u_j^{n+1} + u_{j-1}^{n+1}}{(\Delta y^*)^2} \quad (49)$$

Simplify by multiplying both sides of the equation by  $\Delta t^*$  and factor out the time-stepping parameter from the spatial term.

$$-ru_{j-1}^{n+1} + (1 - 2r)u_j^{n+1} - ru_{j-1}^{n+1} = u_j^n + \Delta t^* \quad (50)$$

Equation (50) is the finite difference equation for interior points. Apply the boundary conditions from Equations (11) and (12). At  $y^* = 0$ ,

$$\frac{\partial u^*}{\partial y^*} \Big|_{y^*=0} = 0 \rightarrow u_0^{n+1} = u_1^{n+1} \quad (51)$$

So for when  $j = 1$ ,

$$u_0^{n+1} = u_1^{n+1} \rightarrow -ru_0^{n+1} + (1 + 2r)u_1^{n+1} - ru_2^{n+1} = u_1^n + \Delta t^* \quad (52)$$

Which simplifies down to

$$(1 + r)u_1^{n+1} - ru_2^{n+1} = u_1^n + \Delta t^* \quad (53)$$

At  $y^* = 1$ ,

$$u_{N_y}^{n+1} = 0 \quad (54)$$

So for when  $j = N_y - 1$ ,

$$-ru_{N_y-2}^{n+1} + (1 + 2r)u_{N_y-1}^{n+1} = u_{N_y-1}^n + \Delta t^* \quad (55)$$

Substituting all interior nodes into the finite difference equation and applying the boundary conditions results in a tridiagonal system of linear equations for  $u_j^{n+1}$  at each time step. This system can be written in matrix form. The full linear system for the interior points at each time step can be written in matrix form as:

$$\begin{bmatrix} b_1 & c_1 & 0 & \cdots & 0 & 0 \\ a_2 & b_2 & c_2 & \cdots & 0 & 0 \\ 0 & a_3 & b_3 & \cdots & 0 & 0 \\ \vdots & \vdots & \vdots & \ddots & \vdots & \vdots \\ 0 & 0 & 0 & \cdots & b_{N_y-2} & c_{N_y-2} \\ 0 & 0 & 0 & \cdots & a_{N_y-1} & b_{N_y-1} \end{bmatrix} \begin{bmatrix} u_1^{n+1} \\ u_2^{n+1} \\ u_3^{n+1} \\ \vdots \\ u_{N_y-2}^{n+1} \\ u_{N_y-1}^{n+1} \end{bmatrix} = \begin{bmatrix} u_1^n + \Delta t^* \\ u_2^n + \Delta t^* \\ u_3^n + \Delta t^* \\ \vdots \\ u_{N_y-2}^n + \Delta t^* \\ u_{N_y-1}^n + \Delta t^* \end{bmatrix}$$

The system is tridiagonal and can be efficiently solved using the Thomas Algorithm as described in [1]. The flowrate can be approximated numerically using the trapezoidal rule.

$$Q^n \approx 2 \sum_{j=1}^{N_y-1} u_j^n \Delta y^* + \frac{1}{2}(u_0^n + u_{N_y}^n) \Delta y^* \quad (56)$$

The shear stress at the wall ( $y^* = 1, j = N_y$ ) can be approximated by using a backward difference.

$$\tau^n \approx -\frac{u_{N_y}^n - u_{N_y-1}^n}{\Delta y^*} \quad (57)$$

However, since  $u_{N_y} = 0$ , this can be simplified further.

$$\tau^n \approx \frac{u_{N_y-1}^n}{\Delta y^*} \quad (58)$$

### 3.2 Explicit Euler Method

To develop the explicit Euler method to solve Equation (9) with the initial condition in Equation (10) and boundary conditions in Equations (11) and (12), the domain is discretized in the same way as done for the implicit Euler method. A forward difference scheme is used to approximate the time derivative, and a central difference scheme is used to approximate the second spatial derivative.

$$\left. \frac{\partial u^*}{\partial t^*} \right|_j^n \approx \frac{u_j^{n+1} - u_j^n}{\Delta t^*} \quad (59)$$

$$\left. \frac{\partial^2 u^*}{\partial y^*} \right|_j^n \approx \frac{u_{j+1}^n - 2u_j^n + u_{j-1}^n}{(\Delta y^*)^2} \quad (60)$$

Substitute Equations (59) and (60) into Equation (9) and multiplying both sides by  $\Delta t^*$ .

$$u_j^{n+1} = u_j^n + \Delta t^* + r(u_{j+1}^n - 2u_j^n + u_{j-1}^n) \quad (61)$$

This is valid for all interior points  $j = 1, 2, \dots, N_y - 1$ . For the boundary points, apply the boundary conditions to (61).

$$y^* = 0 \rightarrow \left. \frac{\partial u^*}{\partial t^*} \right|_{y^*=0} = 0 \rightarrow u_0^n = u_1^n \quad (62)$$

$$y^* = 1 \rightarrow u_{N_y}^n = 0 \quad (63)$$

$$(64)$$

As stated in [1], the explicit Euler method is conditionally stable. For stability, the time-stepping parameter  $r$  must be

$$r = \frac{\Delta t^*}{(\Delta y^*)^2} \leq \frac{1}{2} \quad (65)$$

The same approximations for flowrate and wall shear stress stated in the implicit method development, Equations (56) and (58) can be used for the explicit method as well.

### 3.3 4th-Order Runge-Kutta Method

To approximate the dimensionless partial differential equation in Equation (9), the equation can be treated as a system of ODEs in time by discretizing the spatial derivative using second-order central differences, while integrating in time using the classical RK4 method. Let the spatial domain be discretized as:

$$y_j^* = j\Delta y^*, \quad j = 0, 1, \dots, N_y, \quad (66)$$

$$u_j^n \approx u^*(y_j^*, t_n^*), \quad (67)$$

with time step size  $\Delta t^*$  and spatial step size  $\Delta y^*$ , and let  $r = \Delta t^*/(\Delta y^*)^2$ . Define the right-hand side function  $f_j(u)$  for each node as:

$$f_j(u) = 1 + \frac{u_{j+1} - 2u_j + u_{j-1}}{(\Delta y^*)^2} \quad (68)$$

Then, the RK4 update proceeds as follows:

1. **Compute  $k_1$ :**

$$k_1 = f(u^n) \quad (69)$$

2. **Compute  $k_2$ :**

$$k_2 = f\left(u^n + \frac{\Delta t^*}{2}k_1\right) \quad (70)$$

3. **Compute  $k_3$ :**

$$k_3 = f\left(u^n + \frac{\Delta t^*}{2}k_2\right) \quad (71)$$

4. **Compute  $k_4$ :**

$$k_4 = f(u^n + \Delta t^*k_3) \quad (72)$$

5. **Update solution:**

$$u^{n+1} = u^n + \frac{\Delta t^*}{6}(k_1 + 2k_2 + 2k_3 + k_4) \quad (73)$$

Boundary conditions from Equations (11) and (12) are enforced at each stage of  $k_i$ , such that:

$$u_0 = u_1 \quad (74)$$

$$u_{N_y} = 0 \quad (75)$$

This method provides fourth-order accuracy in time and second-order accuracy in space, assuming that the spatial derivative is computed using a central difference operator. The same approximation as developed in the implicit method section for flowrate and wall shear stress can also be applied to the RK4 method.

## 4 Results and Discussion

The results of each given method include the time development of the velocity profile, the flowrate versus time, and the wall shear stress versus time.

### 4.1 Comparison of Methods

The exact solution of the governing equation does not have a stability requirement and is inherently exact for any value of  $r$ . The implicit Euler method is unconditionally stable. The explicit Euler is conditionally stable. For the explicit Euler method,  $r \leq 1/2$ . To directly compare the results of each of the methods, a value of  $r = 0.4$  is used. The value of  $\Delta y^*$  is chosen to be 0.05, which by Equation (43) makes  $\Delta t^* = 0.001$ . For the exact solution, since it is independent of  $r$ , let  $N = 500$  for the summation so that an adequate number of terms are in the infinite summation. For the sake of visibility, the velocity profile is plotted every  $\Delta t^* = 0.1$  in the range  $0 \leq t^* \leq 3$ .

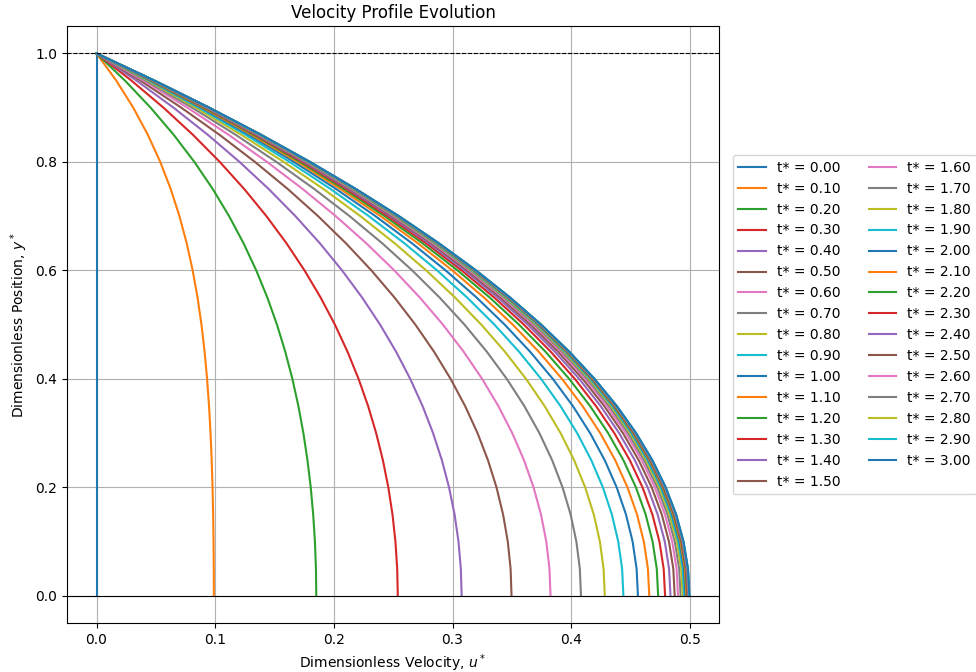


Figure 1: Exact Solution, Velocity Profile,  $r = 0.4$ .

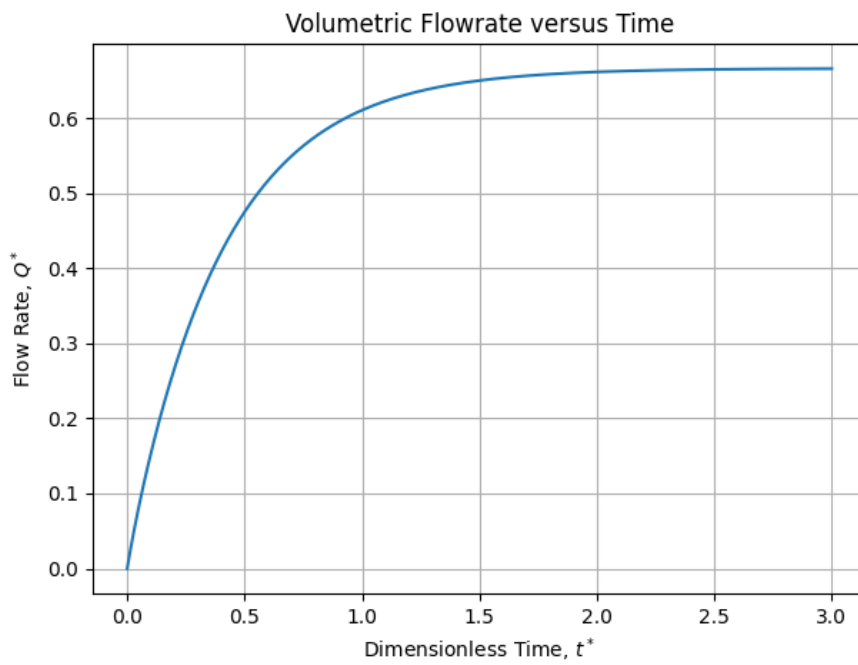


Figure 2: Exact Solution, Volumetric Flowrate,  $r = 0.4$ .

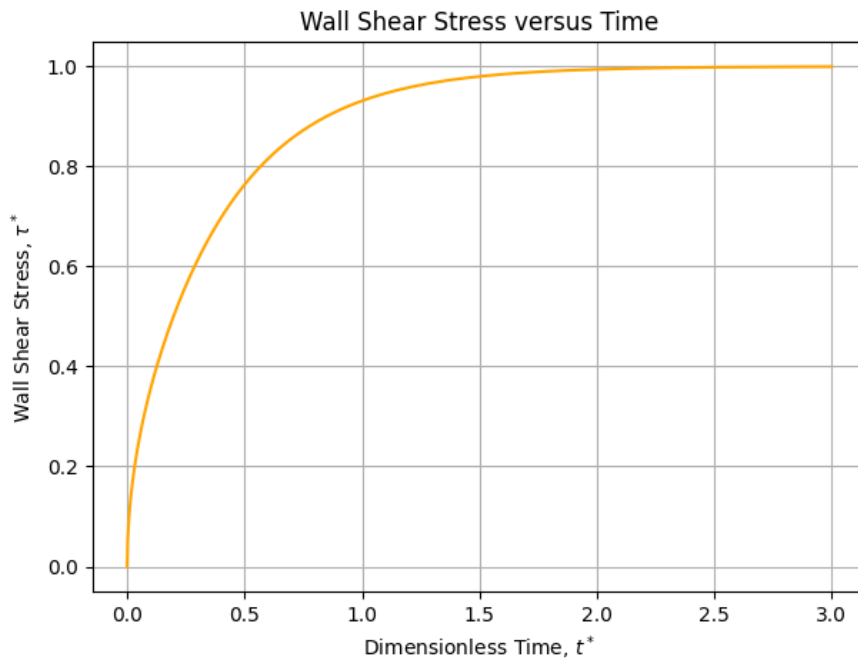


Figure 3: Exact Solution, Wall Shear Stress,  $r = 0.4$ .

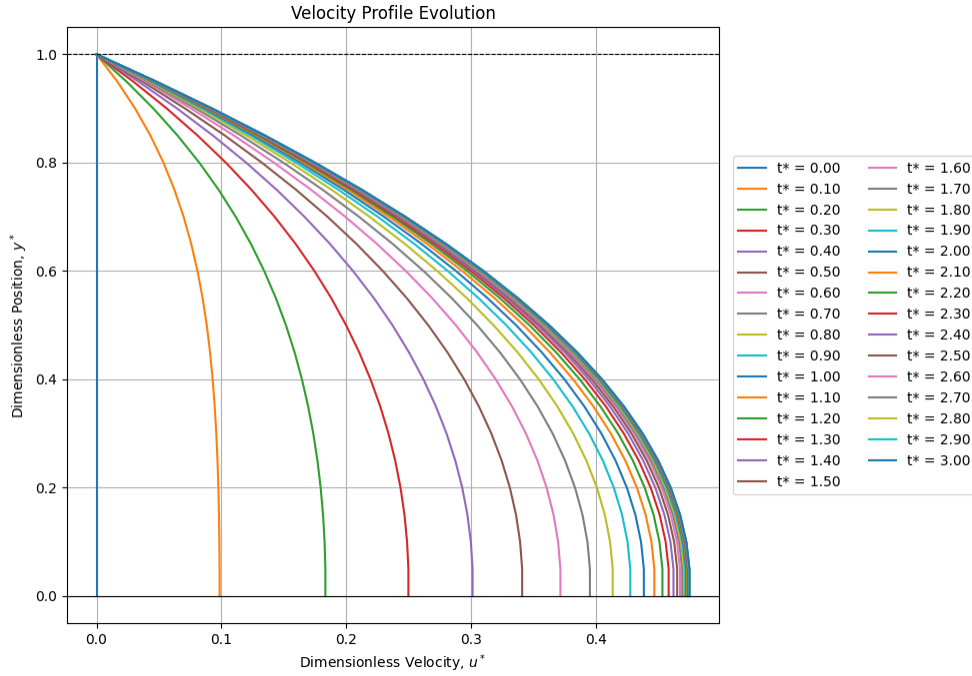


Figure 4: Implicit Euler Solution, Velocity Profile,  $r = 0.4$ .

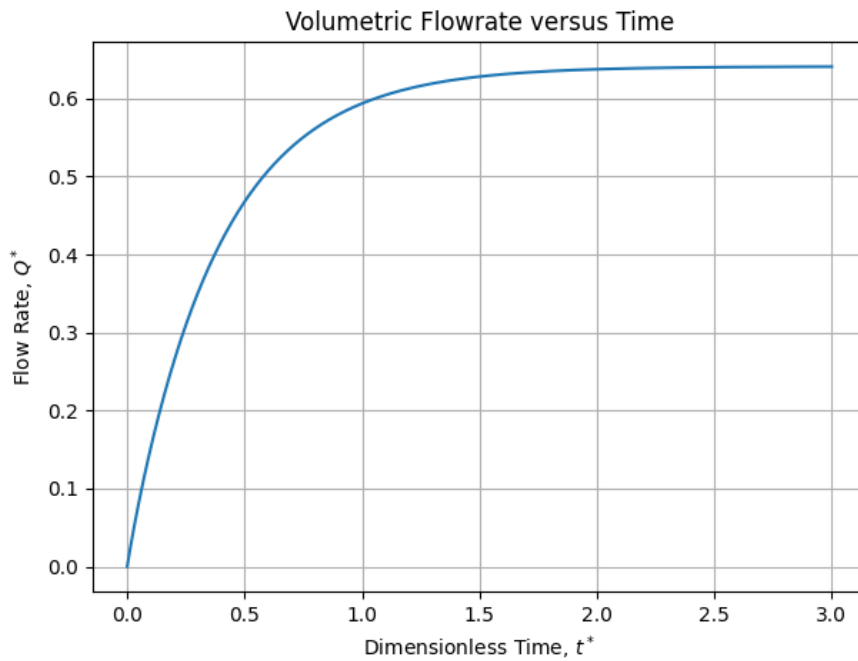


Figure 5: Implicit Euler Solution, Volumetric Flowrate,  $r = 0.4$ .

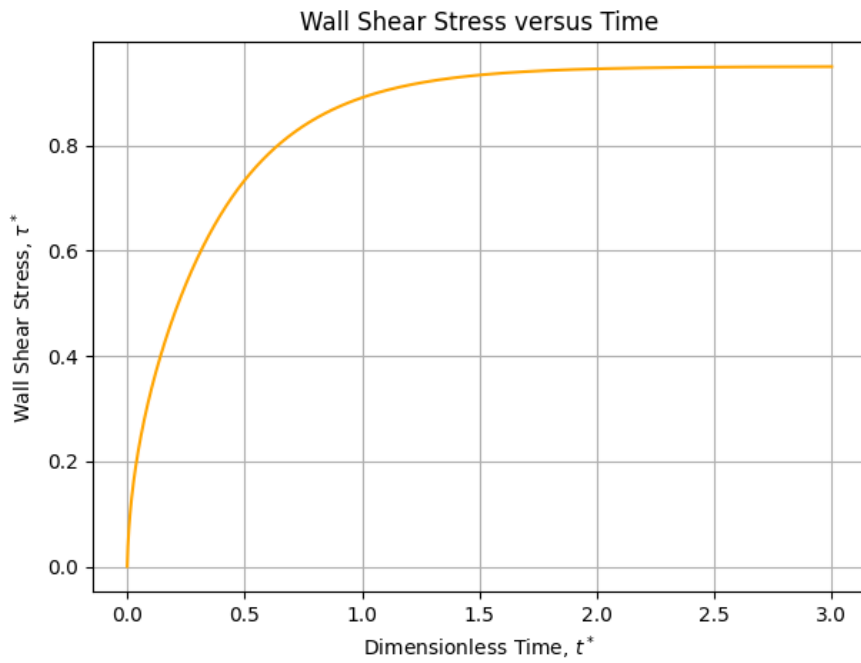


Figure 6: Implicit Euler Solution, Wall Shear Stress,  $r = 0.4$ .

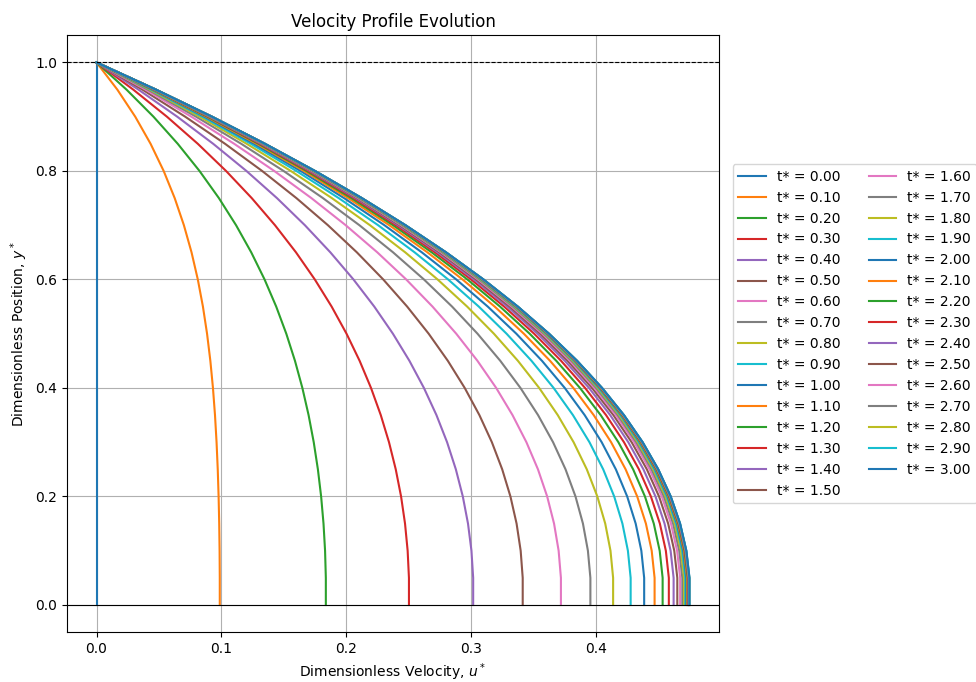


Figure 7: Explicit Euler Solution, Velocity Profile,  $r = 0.4$ .

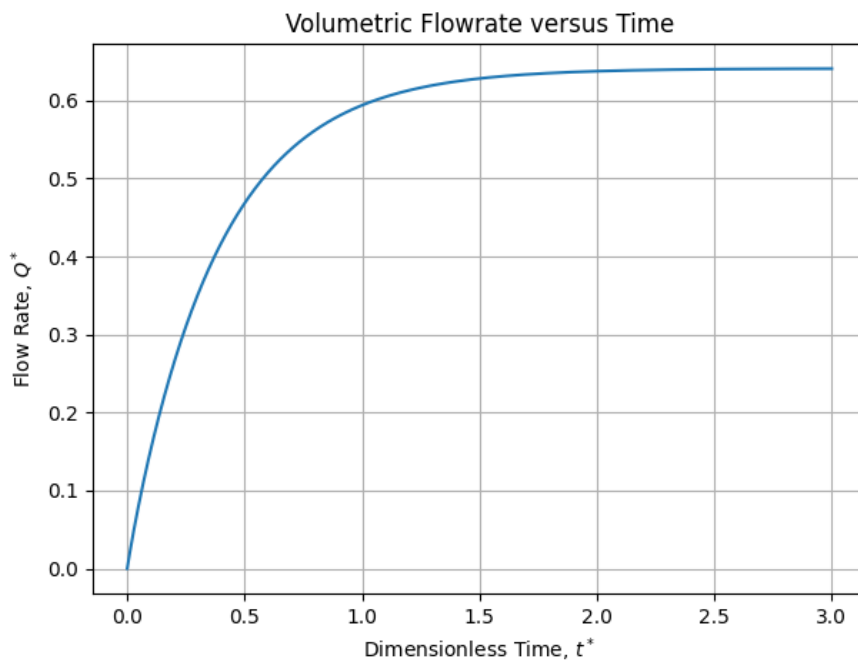


Figure 8: Explicit Solution, Volumetric Flowrate,  $r = 0.4$ .

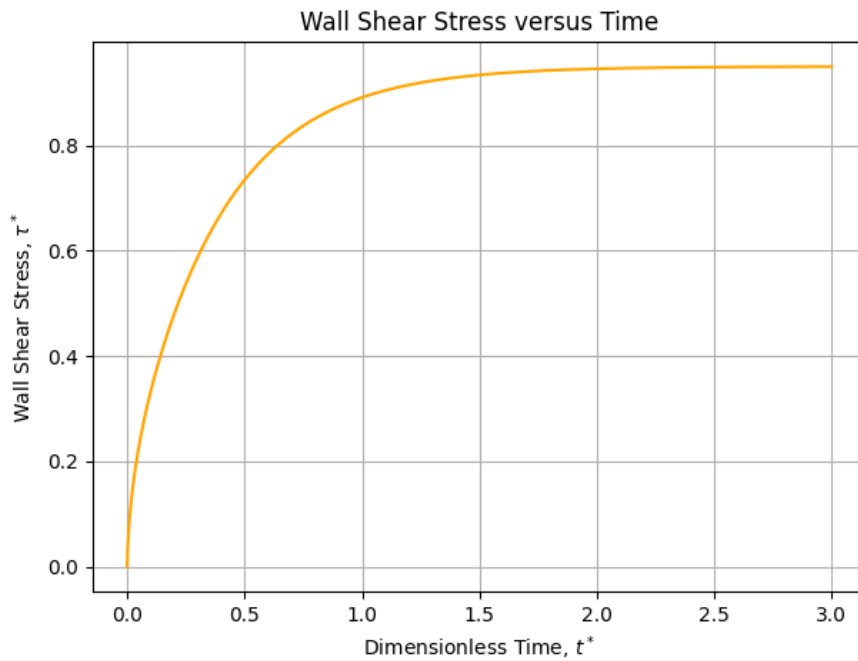


Figure 9: Explicit Solution, Wall Shear Stress,  $r = 0.4$ .

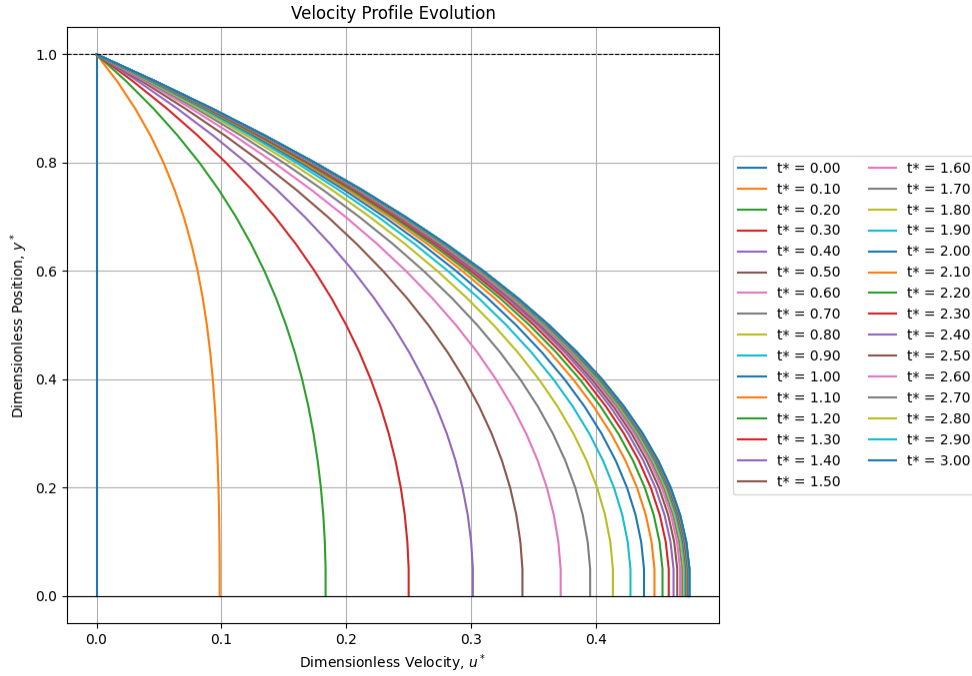


Figure 10: RK4 Solution, Velocity Profile,  $r = 0.4$ .

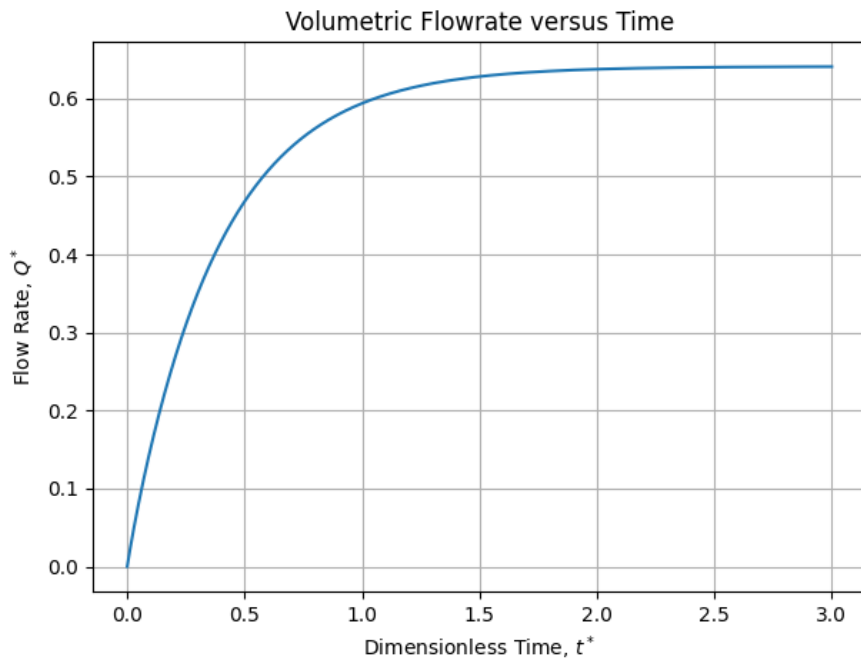


Figure 11: RK4 Solution, Flowrate,  $r = 0.4$ .

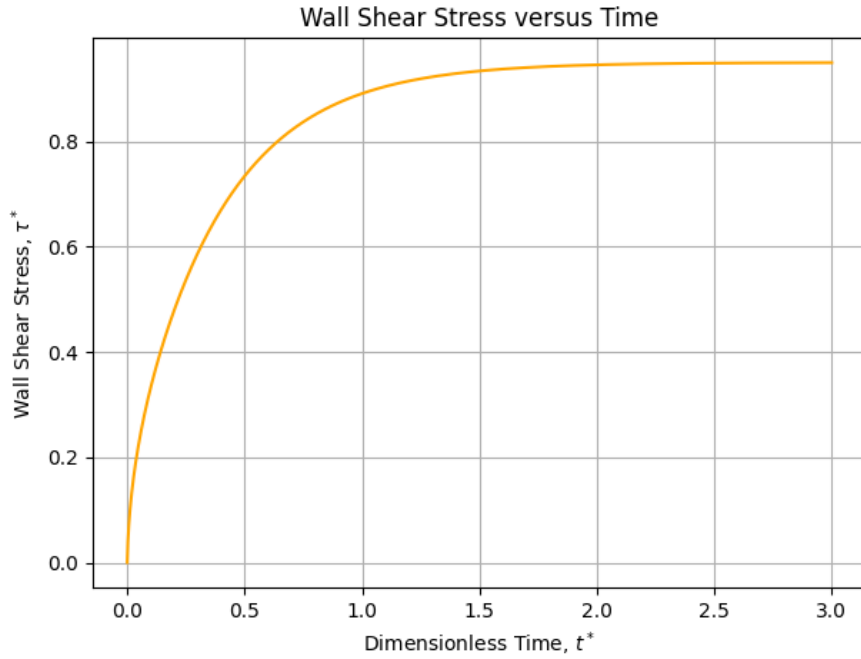


Figure 12: RK4 Solution, Wall Shear Stress,  $r = 0.4$ .

Considering the velocity profile evolutions in Figures 1, 4, 7, and 10 all four methods capture the general trend that the velocity profile starts at rest and gradually evolves to a parabolic steady state. The boundary conditions are clearly respected, that the wall is no-slip and there is a symmetry at  $y^* = 0$ . The exact solution velocity profile in Figure 1 shows perfect, smooth profiles. This serves as a reference for the numerical methods. The implicit Euler velocity profile in Figure 4 is very close to the exact solution, but there is some numerical diffusion at earlier time values. The explicit Euler velocity profile in Figure 7 is slightly more diffusion than the implicit solution. This is due to the fact that  $r = 0.4$  is very close to the stability limit, therefore the accuracy is slightly lower compared to the implicit Euler method and the exact solution. All of the numerical methods underestimate the exact solution due to the high value of  $\Delta y^*$ . The effects of changing  $\Delta y^*$  and  $\Delta t^*$  are discussed in the next sections.

Considering the volumetric flowrates in Figures 2, 5, and 8, all curves asymptotically approach a steady value as  $t^* \rightarrow 3$ . The trend is exponential-like growth, and is consistent across all methods. The exact solution flowrate in Figure 2 is the smoothest, and has the fastest convergence to steady state. The implicit Euler flowrate in Figure 5 matches the exact solution closely but with slightly delayed convergence. The explicit Euler flow rate in Figure 8 slightly underestimates the flow rate during the transient region. This is likely due to accumulated error from the lower-order method and numerical diffusion.

Considering the wall shear stresses in Figures 3, 6, and 9, all methods capture the increase in shear stress as the boundary layer develops and eventually stabilizes. The final steady-state value is the same across all three methods. The exact wall shear stress in Figure 3 has the steepest initial rise and fastest convergence. The implicit Euler in Figure 6 is slightly behind

---

the exact solution but otherwise follows the trend in the exact wall shear stress. The explicit Euler wall shear stress in Figure 9 is even more behind compared to the implicit wall shear stress. The slight under prediction in the early transient region is due to stronger smoothing. The implicit Euler method is the better choice for balancing stability and accuracy, and is conditionally stable. The explicit Euler method is valid, but shows more numerical diffusion, especially over long time periods.

## 4.2 Accuracy and Stability Study of Implicit and Explicit Methods

In this section, the effects of changing  $\Delta t^*$ ,  $\Delta y^*$  and  $r$ . Only the velocity profiles of the two methods will be considered, as the velocity profile is the primary quantity that is being solved for, and both flowrate and wall shear stress are derived from velocity. Changes in time and space resolution will be most noticeable in shape and smoothness of the velocity profiles. Numerical diffusion, oscillations, and instabilities can be easily caught. If  $\Delta y^*$  is too large, stair-stepping artifacts will be visible. If  $\Delta t^*$  is too large, temporal drift or lag will be visible. If  $r$  is too large for the explicit method, instability or divergence will be visible. Since the implicit method is unconditionally stable, there will be no significant change in results. By varying  $\Delta y^*$  or  $\Delta t^*$ ,  $r$  is inherently varied, so by varying either of the two step parameters, the effects of varying  $r$  can also be studied.

### 4.2.1 Effects of Varying $\Delta t^*$

To study the effects of varying  $\Delta t^*$ ,  $\Delta y^*$  must be kept constant. Therefore,  $\Delta y^* = 0.01$  and  $r$  will be allowed to change freely, as constraining both  $r$  and  $\Delta y^*$  would result in only one valid  $\Delta t^*$  value.

$\Delta t^*$	$r$
1e-6	0.01
1e-5	0.1
3e-5	0.3
5e-5	0.5
5.5e-5	0.55
7e-5	0.7

Table 1: Varied Values of  $\Delta t^*$  and Corresponding  $r$  Values.

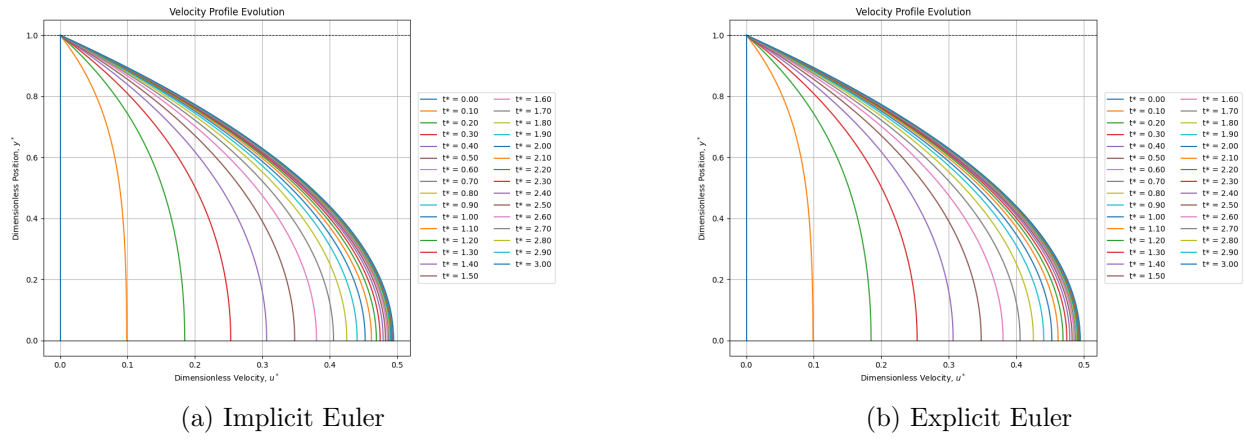


Figure 13: Velocity Profiles at  $\Delta t^* = 1e-6$

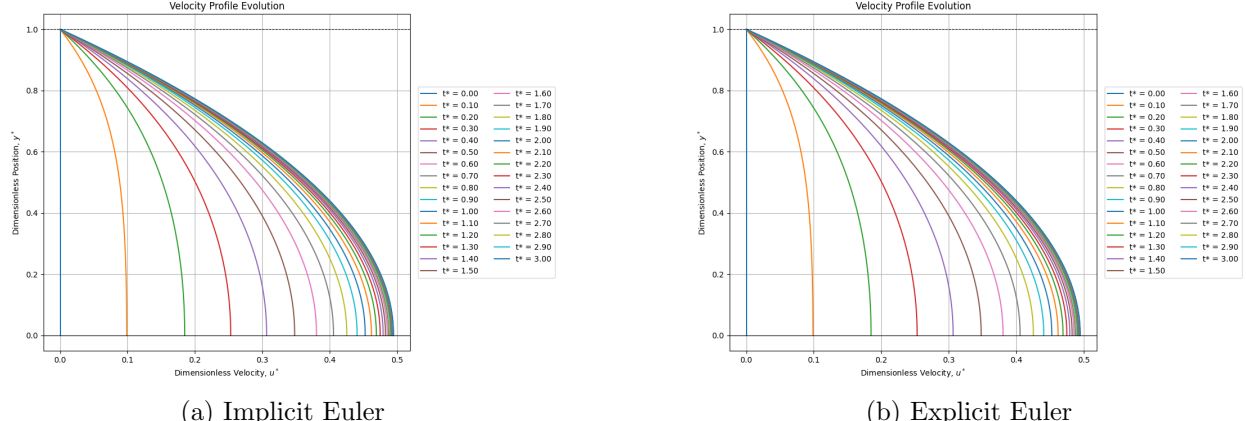


Figure 14: Velocity Profiles at  $\Delta t^* = 3e-5$

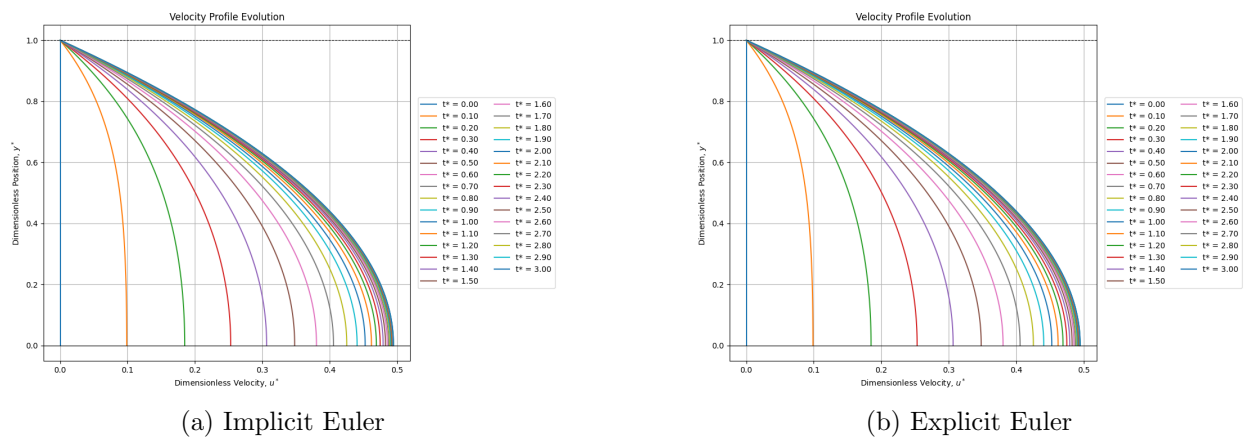


Figure 15: Velocity Profiles at  $\Delta t^* = 5e-5$

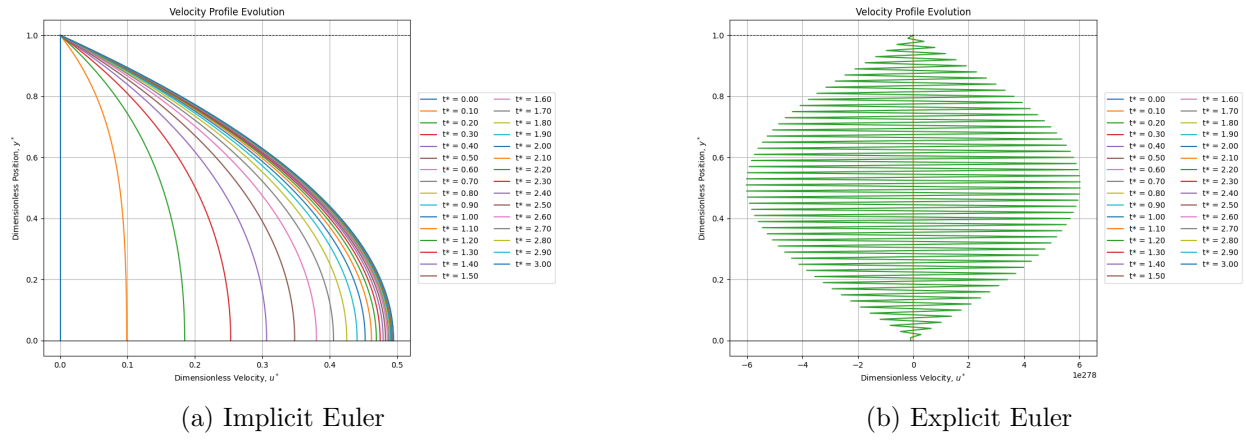


Figure 16: Velocity Profiles at  $\Delta t^* = 5.5\text{e}{-5}$

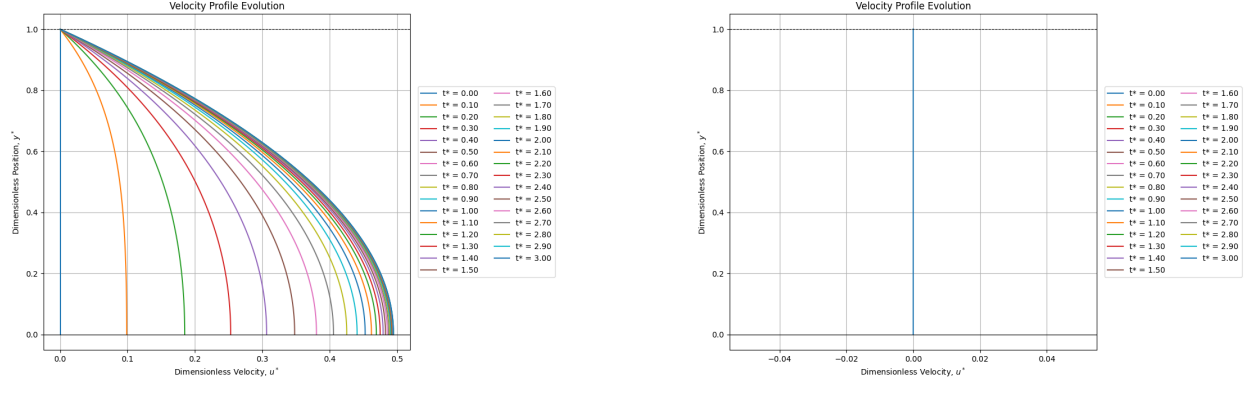


Figure 17: Velocity Profiles at  $\Delta t^* = 7\text{e}{-5}$

From the figures above, it can be seen that the implicit Euler method is stable at all of the chosen values of  $\Delta t^*$ , because it is unconditionally stable. In contrast, the explicit Euler method produces a valid solution up to  $r = 0.5$ . At  $\Delta t^* = 5.5\text{e}{-5}$ ,  $r = 0.55$ , the method becomes unstable and oscillates. This is due to the fact that the explicit Euler method is conditionally stable to  $r \leq 0.5$ . At  $\Delta t^* = 7\text{e}{-5}$ ,  $r = 0.7$ , the oscillations cease and the method becomes completely broken down. Unless a very high value for  $\Delta t^*$  is used the solution is always accurate, it is simply a matter of resolution. Both the implicit and explicit Euler methods are accurate with each value of  $\Delta t^*$ , until the explicit Euler method breaks down when  $r \geq 0.5$ . The methods underestimate compared to the exact solution, but this is due to the chosen value for  $\Delta y^*$ , which is discussed in the following sections.

#### 4.2.2 Effects of Varying $\Delta y^*$

To study the effects of varying  $\Delta y^*$ ,  $\Delta t^*$  must be kept constant. Therefore,  $\Delta t^* = 0.0001$  and  $r$  will be allowed to change freely, as constraining both  $r$  and  $\Delta t^*$  would result in only

one valid  $\Delta y^*$  value.

$\Delta y^*$	$r$
0.5	4e-4
0.25	0.0016
0.2	0.0025
0.1	0.01
0.075	0.0178
0.05	0.04
0.02	0.25
0.015	0.4444
0.0142	0.496
0.014	0.5102
0.01	1

Table 2: Varied Values of  $\Delta y^*$  and Corresponding  $r$  Values.

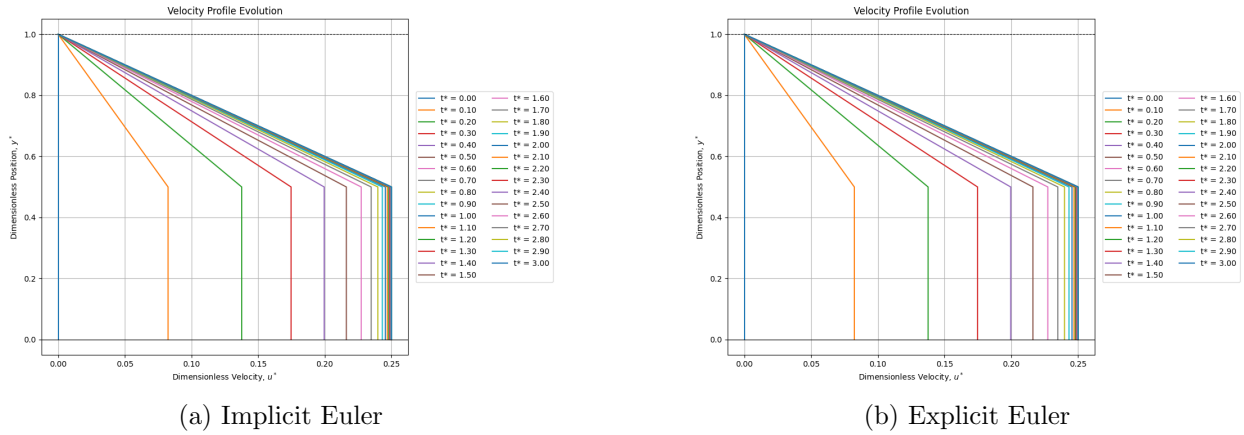


Figure 18: Velocity Profiles at  $\Delta y^* = 0.5$

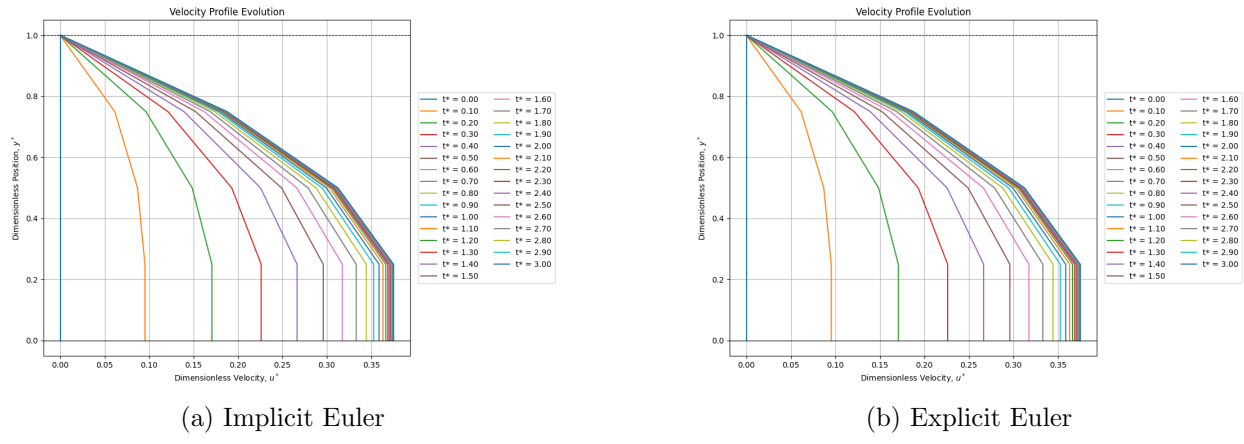


Figure 19: Velocity Profiles at  $\Delta y^* = 0.25$

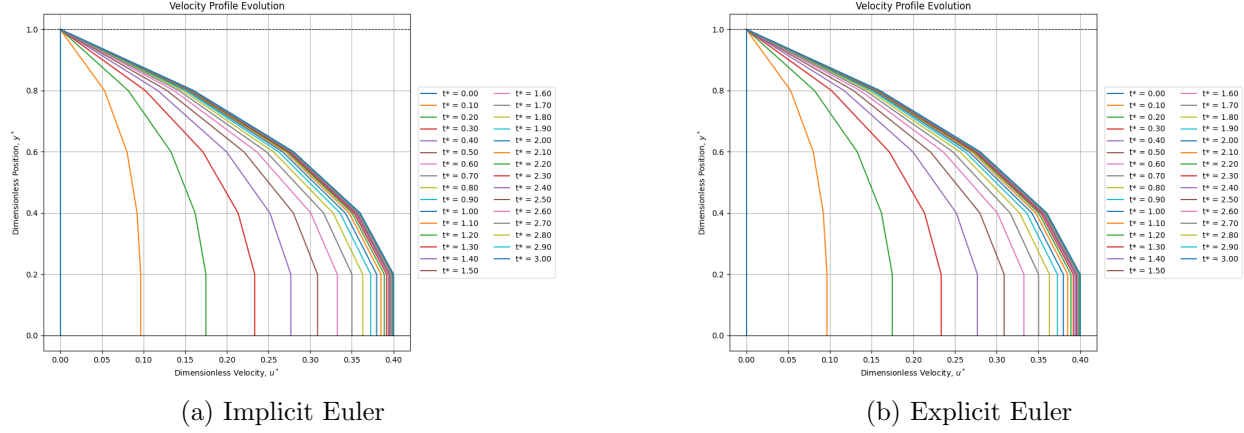


Figure 20: Velocity Profiles at  $\Delta y^* = 0.2$

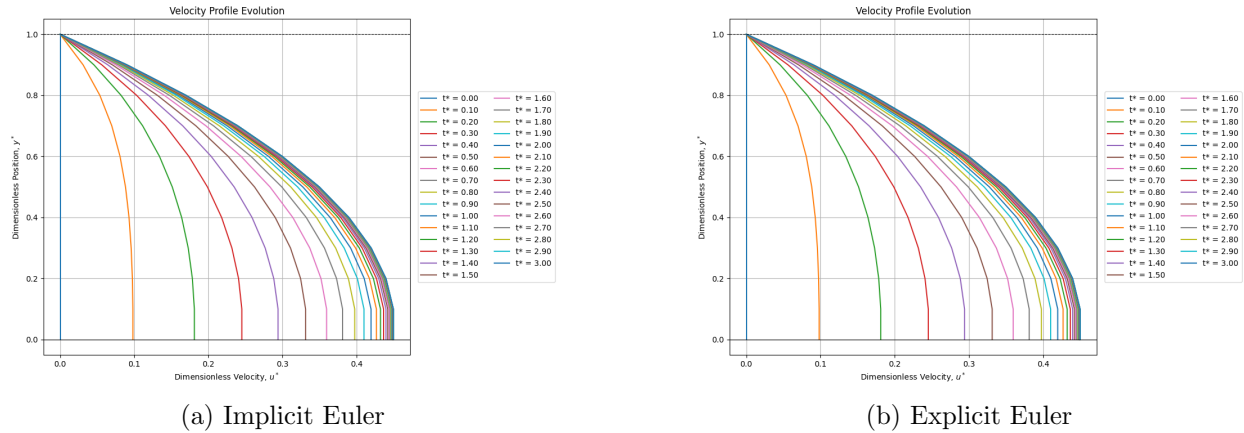


Figure 21: Velocity Profiles at  $\Delta y^* = 0.1$

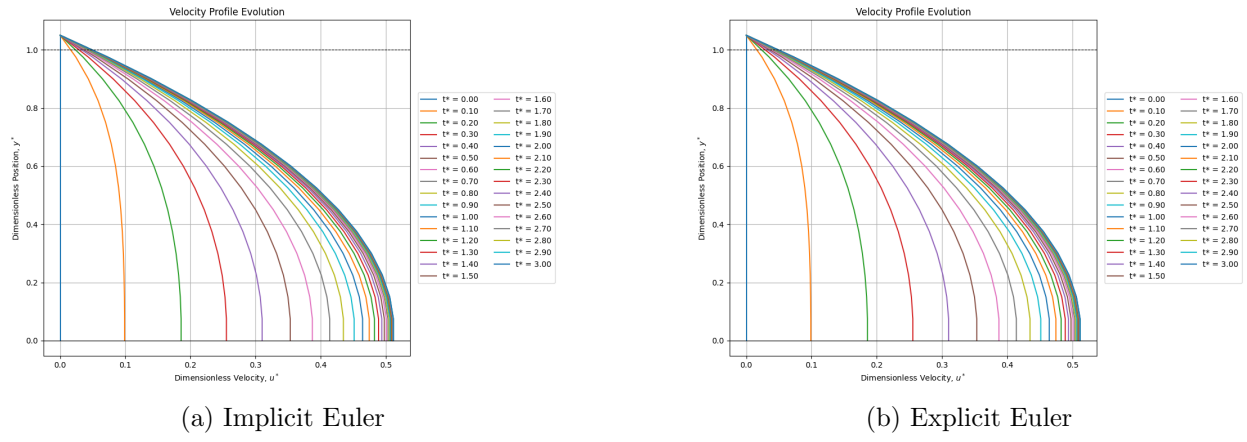


Figure 22: Velocity Profiles at  $\Delta y^* = 0.075$

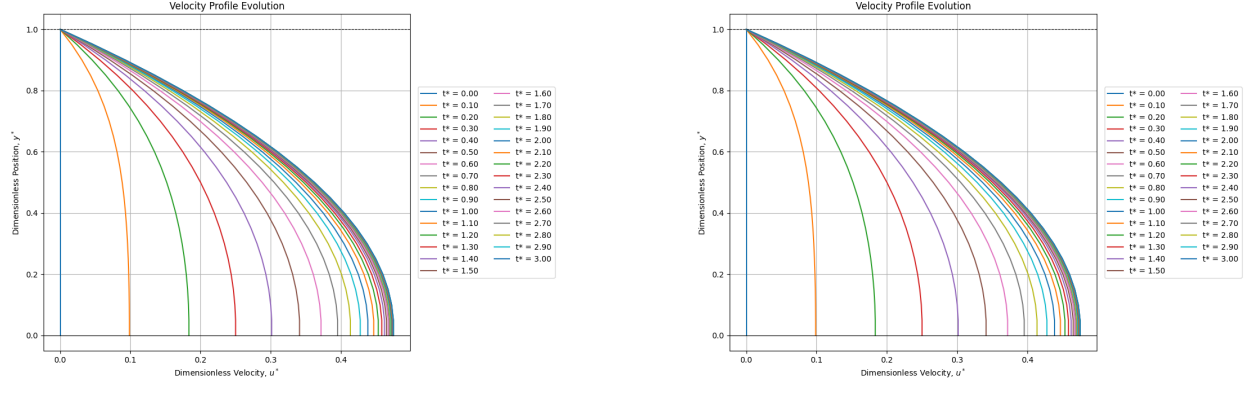


Figure 23: Velocity Profiles at  $\Delta y^* = 0.05$

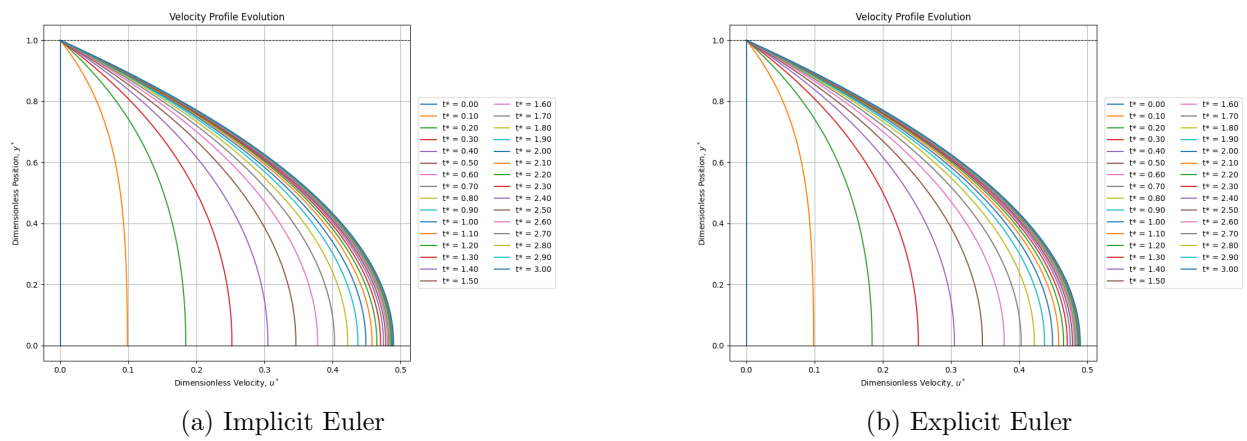


Figure 24: Velocity Profiles at  $\Delta y^* = 0.02$

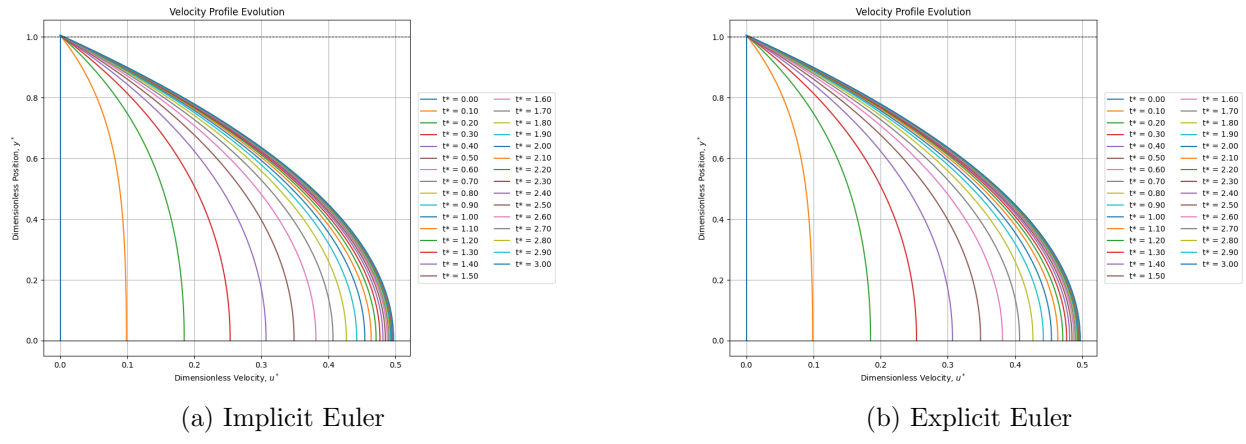


Figure 25: Velocity Profiles at  $\Delta y^* = 0.015$

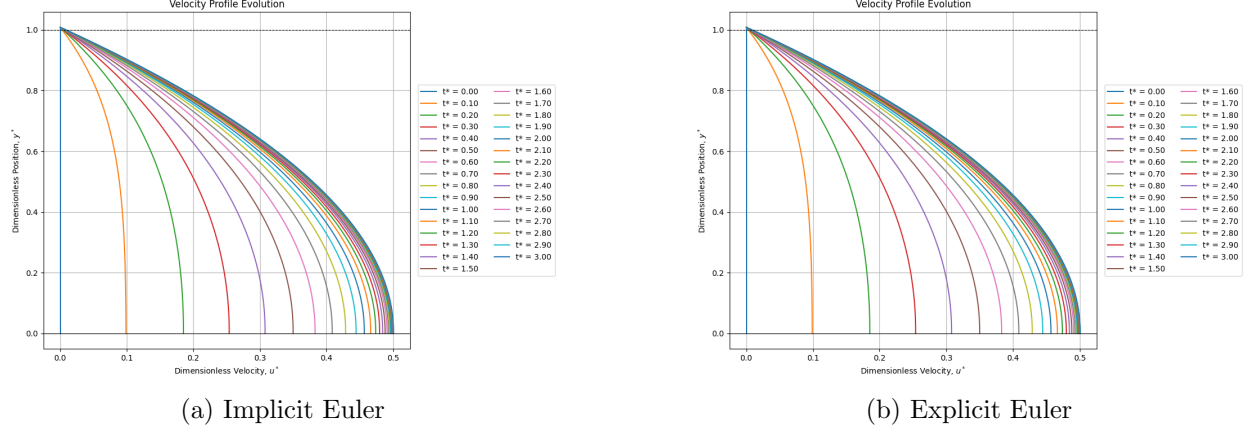


Figure 26: Velocity Profiles at  $\Delta y^* = 0.0142$

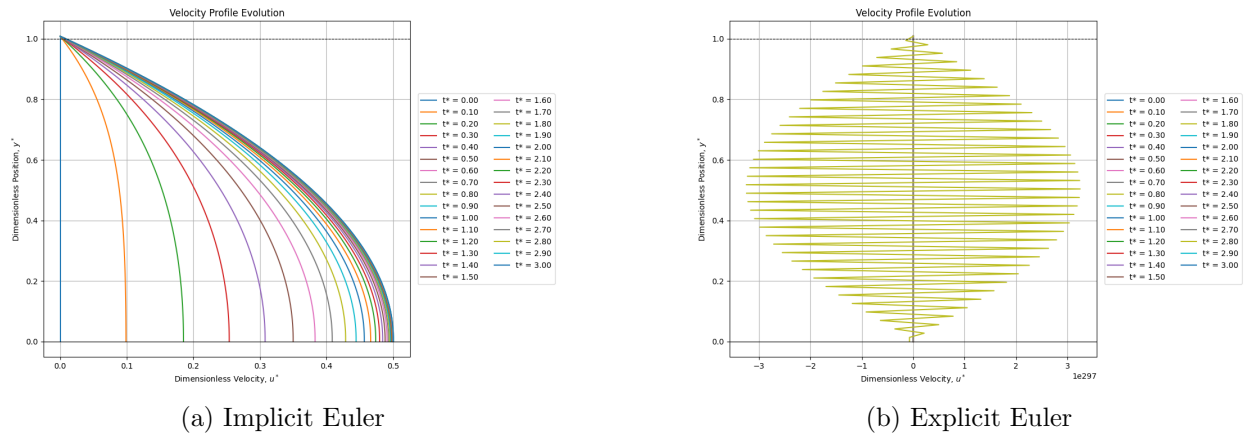


Figure 27: Velocity Profiles at  $\Delta y^* = 0.014$

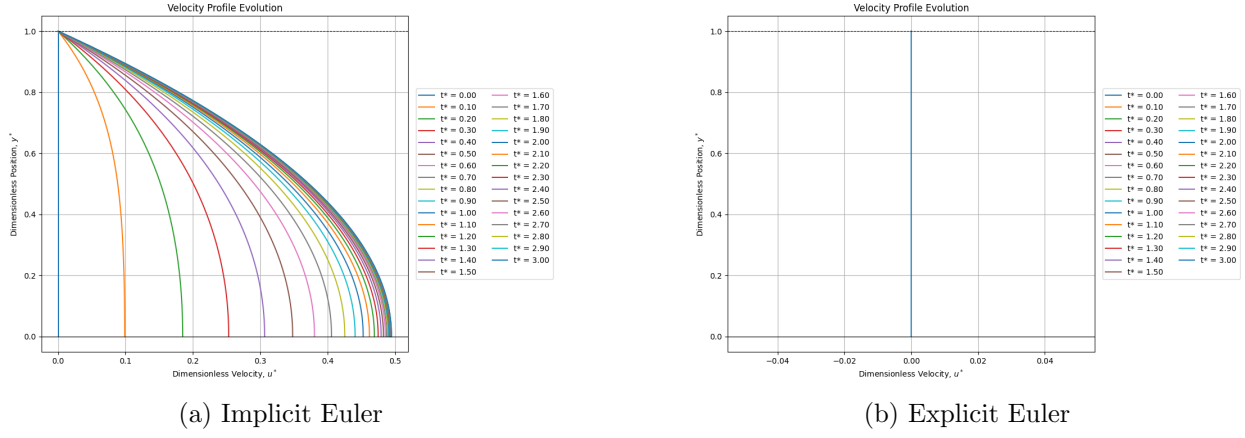


Figure 28: Velocity Profiles at  $\Delta y^* = 0.01$

When  $\Delta y^*$  is very high, stair stepping can be very clearly seen. As  $\Delta y^*$  decreases, the solution smooths out and becomes more accurate. While the implicit method continues to get smoother with lower  $\Delta y^*$ , the explicit method hits its limit when  $r = 0.5$ , where it begins to oscillate before diverging, similarly to when  $\Delta t^*$  was varied. Additionally, when  $\Delta y^*$  is high, the solution is highly inaccurate when compared to the exact solution. Both explicit and implicit Euler methods drastically underestimate the solution until about  $\Delta y^* = 0.075$ , where it overshoots the exact solution. At  $\Delta y^* = 0.05$ , the solution is underestimated again, but further decreases bring both methods closer to the exact solution, until  $r \geq 0.5$ , where the explicit Euler method breaks down.

### 4.3 4th-Order Runge-Kutta Method and Effects of $\Delta t^*$

As shown in the study of implicit and explicit Euler methods, a value of  $\Delta y^* = 0.01$  is adequate to see accurate results. By varying  $\Delta t^*$  and  $r$ , we can see for what range of  $r$  that the RK4 method is stable for.

$\Delta t^*$	$r$
1e-5	0.1
2e-5	0.2
3e-5	0.3
4e-5	0.4
5e-5	0.5
7e-5	0.7

Table 3: Varied Values of  $\Delta t^*$  and Corresponding  $r$  Values.

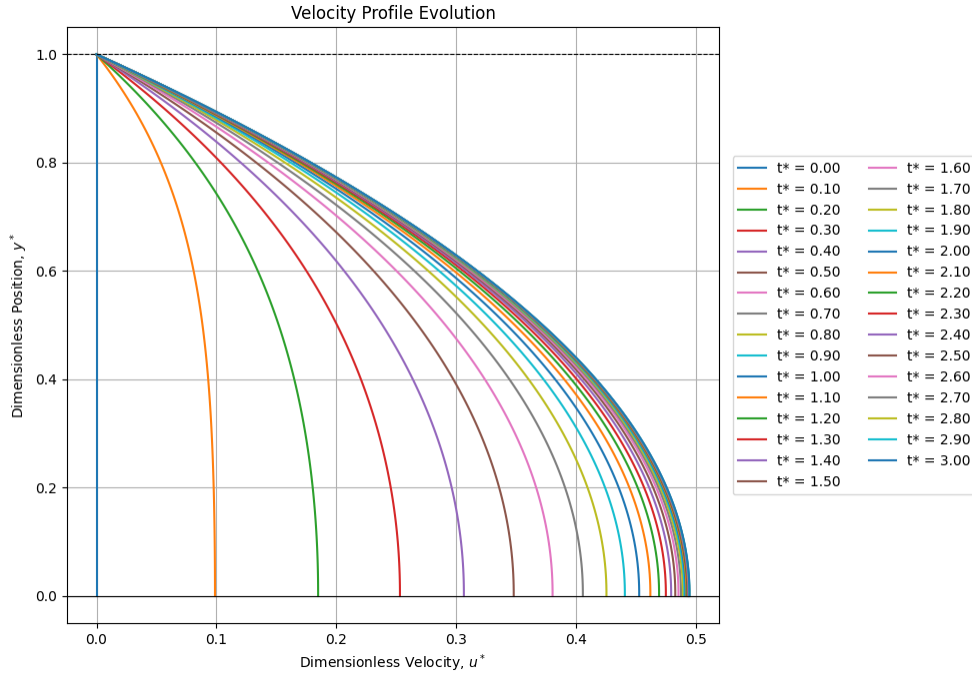


Figure 29: RK4 Method,  $\Delta t^* = 1e - 5$ .

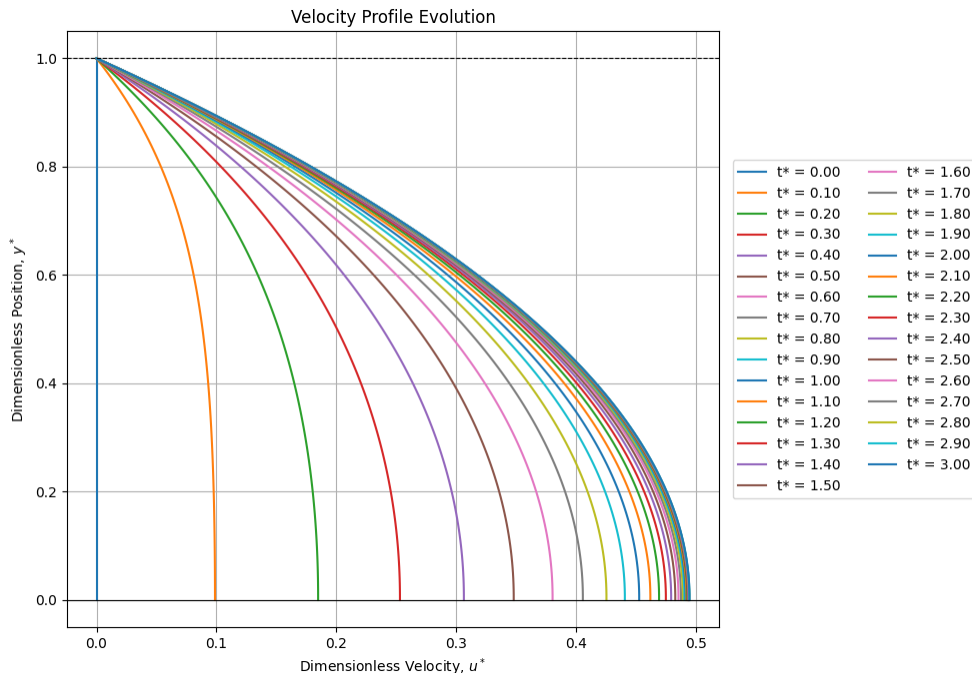


Figure 30: RK4 Method,  $\Delta t^* = 2e - 5$ .

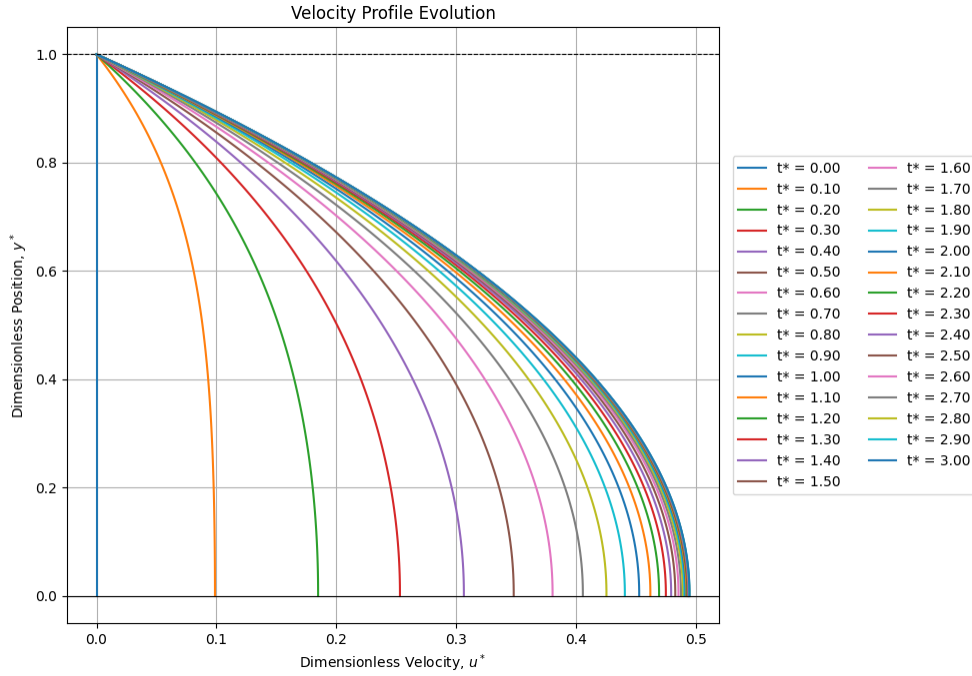


Figure 31: RK4 Method,  $\Delta t^* = 3e - 5$ .

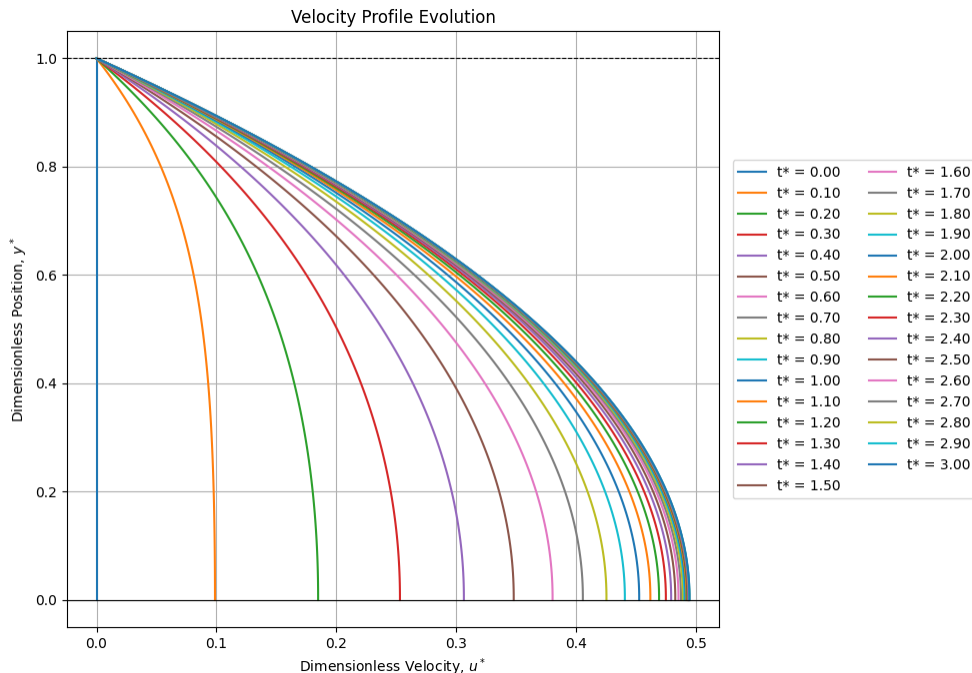


Figure 32: RK4 Method,  $\Delta t^* = 4e - 5$ .

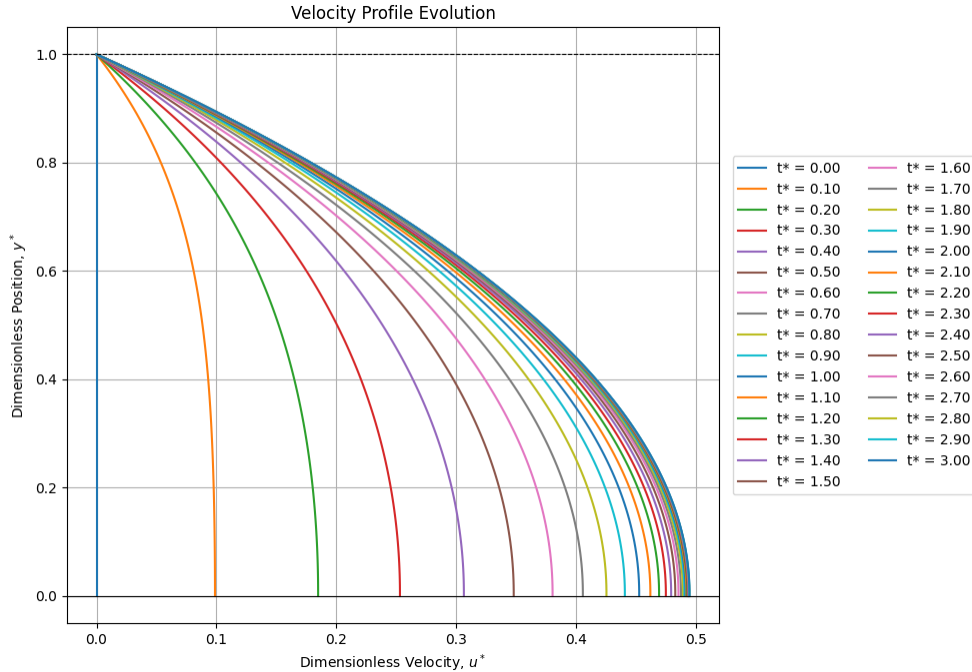


Figure 33: RK4 Method,  $\Delta t^* = 5e - 5$ .

The RK4 method is very accurate, and isn't explicitly effected by varying  $\Delta t^*$ . However, when  $r \geq 0.7$ , the method breaks down completely and  $NaN$  shows up in the solver equations. A smaller timestep could be achieved by raising the spacial step, however this would more quickly sacrifice accuracy as stair stepping would appear. Compared to the exact solution, the RK4 method doesn't reach the maximum velocity value at  $y^* = 0$  of  $u^* = 0.5$ , but it does get close.

## 5 Conclusion

This study investigated the time-developing flow between parallel plates using analytical and numerical approaches. The problem was nondimensionalized to highlight its generality and solved exactly using separation of variables. The analytical solution served as a benchmark for evaluating the performance of the implicit Euler, explicit Euler, and RK4 numerical methods.

Results demonstrated that all three numerical methods correctly captured the transient evolution of the velocity profile and asymptotic approach to the steady-state parabolic distribution. The implicit Euler method showed reliable stability and acceptable accuracy, even for relatively large timesteps. The explicit Euler method, while straightforward, was sensitive to the timestep and became unstable for  $r \geq 0.5$ , as predicted. The RK4 method displayed high accuracy and resolution but became unstable for high values of  $r$ , suggesting a stricter stability constraint than for implicit methods.

Grid sensitivity analysis revealed that both spatial and temporal resolutions significantly impact numerical accuracy. Reducing  $\Delta y^*$  and  $\Delta t^*$  improved results but increased compu-

---

tational cost. The study concludes that implicit methods offer robustness, while higher-order schemes like RK4 can be advantageous when sufficient resolution and stability conditions are maintained.

Future work could extend this analysis to include adaptive time-stepping schemes, non-constant pressure gradients, or more complex geometries. These additions would further align the simulation with real-world engineering flows where transient effects dominate.

## 6 References

### References

- [1] J. H. Ferziger and M. Peric, *Computational Methods for Fluid Dynamics*, Springer, 2001.